The EMBO Journal (2009) 28, 1637–1643 | © 2009 European Molecular Biology Organization | All Rights Reserved 0261-4189/09
www.embojournal.org

THE EMBO JOURNAL

Inter-subunit interaction of gastric H^+,K^+-ATPase prevents reverse reaction of the transport cycle

Kazuhiro Abe[1], Kazutoshi Tani[1], Tomohiro Nishizawa[1,2] and Yoshinori Fujiyoshi[1,*]

[1]Department of Biophysics, Faculty of Science, Kyoto University, Kyoto, Japan and [2]Research Fellow of the Japan Society for the Promotion of Science, Kyoto University, Kyoto, Japan

The gastric H^+,K^+-ATPase is an ATP-driven proton pump responsible for generating a million-fold proton gradient across the gastric membrane. We present the structure of gastric H^+,K^+-ATPase at 6.5 Å resolution as determined by electron crystallography of two-dimensional crystals. The structure shows the catalytic α-subunit and the non-catalytic β-subunit in a pseudo-E_2P conformation. Different from Na^+,K^+-ATPase, the N-terminal tail of the β-subunit is in direct contact with the phosphorylation domain of the α-subunit. This interaction may hold the phosphorylation domain in place, thus stabilizing the enzyme conformation and preventing the reverse reaction of the transport cycle. Indeed, truncation of the β-subunit N-terminus allowed the reverse reaction to occur. These results suggest that the β-subunit N-terminus prevents the reverse reaction from E_2P to E_1P, which is likely to be relevant for the generation of a large H^+ gradient *in vivo* situation.

The EMBO Journal (2009) **28,** 1637–1643. doi:10.1038/emboj.2009.102; Published online 23 April 2009
Subject Categories: membranes & transport; structural biology
Keywords: cryo-electron microscopy; membrane protein structure; P-type ATPase; two-dimensional crystal

Introduction

Acid secretion by the human stomach results in a median diurnal pH of 1.4. This very large ($>10^6$-fold) H^+ gradient, the highest ion gradient known in mammalian tissues, is generated by the H^+,K^+-ATPase (Ganser and Forte, 1973; Wolosin, 1985), which uses the hydrolysis of one ATP molecule to catalyse the electroneutral exchange of two luminal potassium ions for two cytoplasmic protons. The vectorial ion transport is accomplished by cyclical conformational changes of the enzyme between its two main reaction states, E_1 and E_2. The cytoplasmic-open E_1 and luminal-open E_2 states have high affinity for H^+ and K^+, respectively (Figure 1A) (Rabon and Reuben, 1990). During the transport cycle, an aspartic acid in the conserved DKTG sequence is reversibly auto-phosphorylated to form phosphoenzyme intermediates (EPs), a hallmark of members of the P-type ATPase family (Post and Kume, 1973). The H^+,K^+-ATPase consists of two subunits. The catalytic α-subunit (110 kDa) is homologous to the other ion-motive P2-type ATPases (Palmgren and Axelsen, 1998), such as the Na^+,K^+-ATPase and the sarcoplasmic reticulum Ca^{2+}-ATPase (SERCA). It is composed of 10 transmembrane (TM) helices, in which the ion-binding sites are located, and a large cytoplasmic domain that catalyses ATP hydrolysis. The β-subunit is a type II single-span membrane protein (core MW 35 kDa) with a short N-terminal cytoplasmic tail (~36 residues) and a large C-terminal ectodomain (~230 residues), involved in correct membrane integration and targeting of the complex to the cell surface (Chow and Forte, 1995).

Among the well-studied P2-type ATPases, the gastric H^+,K^+-ATPase is known to have a strong preference for the E_2P state (Figure 1A). Although both Na^+,K^+-ATPase and H^+,K^+-ATPase are predominantly in the E_2P state under physiological conditions, the reverse reaction from E_2P to E_1P is characteristically prohibited in H^+,K^+-ATPase (Rabon *et al*, 1982; Helmich-de Jong *et al*, 1985). Therefore, a mechanism must exist that prevents the reverse reaction and thus avoids inefficient transport and reflux of cations. Despite considerable interest in the function of this clinically important membrane protein, and in contrast to recent progress in structural studies of related P-type ATPases (Toyoshima *et al*, 2000; Morth *et al*, 2007; Olesen *et al*, 2007; Pedersen *et al*, 2007), structural information on the gastric H^+,K^+-ATPase has thus far been missing. Using electron crystallography of two-dimensional (2D) crystals (Fujiyoshi, 1998), we present here the first three-dimensional (3D) structure of an intact gastric H^+,K^+-ATPase in the lipid membrane. Our structure reveals an unexpected interaction between the N-terminus of the β-subunit and the phosphorylation domain of the α-subunit. On the basis of functional analyses of β-subunits with N-terminal deletions, the observed interaction contributes to the inherent E_2P preference of H^+,K^+-ATPase, which would be important for the prevention of the reverse reaction of the transport cycle.

Results and discussion

Overall structure of the H^+,K^+-ATPase in the membrane at 6.5 Å resolution

H^+,K^+-ATPase was purified from pig gastric mucosa and reconstituted into 2D crystals with dioleoylphosphatidylcholine (Figure 1B; Supplementary Figure S1 and Table S1). The crystalline membrane sheets consist of two membrane layers and are 320 Å thick. The asymmetric unit contains one H^+,K^+-ATPase αβ-protomer, and αβ-protomers in the two-membrane layers are related to each other by a two-fold screw axis (Figure 1C). αβ-protomers in the same membrane do not form direct interactions, so that all crystal contacts

*Corresponding author. Department of Biophysics, Faculty of Science, Kyoto University, Oiwake, Kitashirakawa, Sakyo-ku, Kyoto 606-8502, Japan. Tel.: +81 75 753 4215; Fax: +81 75 753 4218;
E-mail: yoshi@em.biophys.kyoto-u.ac.jp

Received: 7 January 2009; accepted: 10 March 2009; published online: 23 April 2009

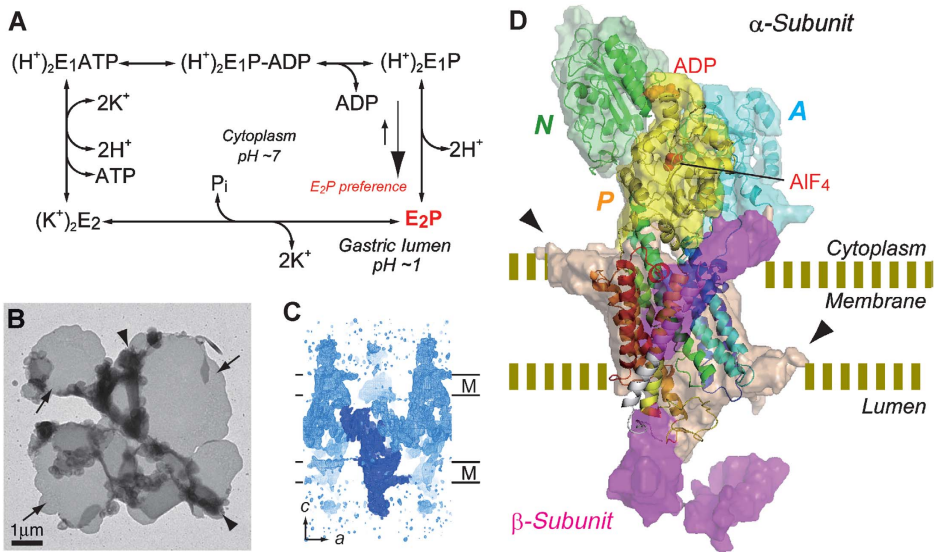

Figure 1 Cryo-EM structure of gastric H^+,K^+-ATPase at 6.5 Å resolution. (**A**) Reaction scheme of the ion transport cycle. The equilibrium between the E_1P and E_2P states of the gastric H^+,K^+-ATPase is largely shifted towards the E_2P state during the phosphorylation reaction (E_2P preference). In our 2D crystals grown in the presence of AlF_4 and ADP, the H^+,K^+-ATPase adopts a pseudo-E_2P state (shown in red). (**B**) Negatively stained 2D crystal of the H^+,K^+-ATPase (arrow) with small amounts of aggregation (arrowhead). (**C**) The density map of the H^+,K^+-ATPase 2D crystal contoured at 1.0 σ shows that the 2D crystals consist of two membrane layers (indicated as M). One αβ-protomer is shown as solid surface representation (dark blue). (**D**) Surface representation of the extracted density map (see Materials and methods) of an H^+,K^+-ATPase αβ-protomer with the fit homology model in ribbon representation. Colour code of the density map: N domain, green; A domain, cyan; P domain, yellow; TM domain of the α-subunit, wheat; β-subunit, magenta. Colour code of the homology model: N, A and P domains have the same colour as the density map; TM helices M1–M10 of the α-subunit, gradual change from M1 (blue) to M10 (red); TM helix of β-subunit, white. The dotted lines indicate the probable position of the lipid head group, resulting total thickness of approximately 35 Å, which is based on the densities protruding perpendicular from the TM domain (arrowheads). The bound ADP and AlF_4 molecules are shown as red spheres.

are mediated by the cytoplasmic domains of protomers in adjoining membranes, with the luminal portions of the protomers protruding from the outer surfaces of the crystals (Figure 1C).

In the 6.5 Å map analysed by electron crystallography, the individual domains of the H^+,K^+-ATPase are well resolved, revealing an overall structure similar to those of other P-type ATPases (Toyoshima *et al*, 2000; Morth *et al*, 2007; Pedersen *et al*, 2007) (Figure 1D; Supplementary Movie S1). The characteristic cytoplasmic domain, consisting of the actuator (A), nucleotide-binding (N) and phosphorylation (P) domains, is connected to the TM domain, which contains the 10 TM helices (M1–M10) of the α-subunit and the single TM helix contributed by the β-subunit. The overall fold is similar to that of the Na^+,K^+-ATPase multi-complex, which includes a large density at the luminal side representing the β-subunit ectodomain (Morth *et al*, 2007). Interestingly, we observed densities protruding perpendicular to the TM helices (Figure 1D, arrowheads) near the M3–M4 loop on the luminal side and the M8–M9 loop on the cytoplasmic side, which may represent the surface of the lipid membrane. Such lipid density has been observed earlier in EM maps obtained with tubular crystals of membrane proteins (Zhang *et al*, 1998; Miyazawa *et al*, 2003). The distance between the two layers (approximately 35 Å) is close to that of lipid bilayers observed in other 2D crystals (Gonen *et al*, 2005). Both the large atomic number of the phosphorus in the lipid head groups as well as the high completeness of our data set (which includes data from specimens tilted up to 70°) may have contributed to the lipid membrane being visible at this resolution.

The α-subunit

The 2D crystals were grown in the presence of ADP and fluoroaluminate (AlF_4), the same components recently used for the structural analysis of SERCA in the E_1P-ADP state (Toyoshima *et al*, 2004). In contrast to that crystal structure, in our EM map, the A domain is close to the P domain, whereas the N domain is approximately 20 Å far away from the P domain (Figure 2A). The H^+,K^+-ATPase structure presented here is thus closer to that of SERCA in the E_2P transition state (Danko *et al*, 2004; Olesen *et al*, 2007). We confirmed the pseudo-E_2P conformation of the H^+,K^+-ATPase under these conditions by limited trypsin digestion of both the membrane fraction and 2D crystals (Supplementary Figure S2) (Nishizawa *et al*, 2008). These results led us to compare our 6.5 Å EM map of the H^+,K^+-ATPase with the structures of SERCA in the E_2AlF_4 state (Olesen *et al*, 2007) and the Na^+,K^+-ATPase in the $(Rb)_2E_2MgF$ state (Morth *et al*, 2007), both of which mimicking the domain arrangement in a E_2P-like state.

We generated a homology model for the H^+,K^+-ATPase using the Na^+,K^+-ATPase structure as template. The resulting model, which includes residues 36–1033 of the α-subunit and residues 33–77 of the β-subunit, fits well into the EM density map (Figure 1D). The locations of the trypsin cleavage sites (Nishizawa *et al*, 2008) in our homology model are consistent with their susceptibility to the protease (Supplementary Figure S2). We ascribe the density located at the outermost part of the A domain surrounding the N-terminal end of the homology model (Lys36) to the residual N-terminal 35 amino acids of the α-subunit (suggesting double arrowhead in Figure 2A), which include phosphorylation

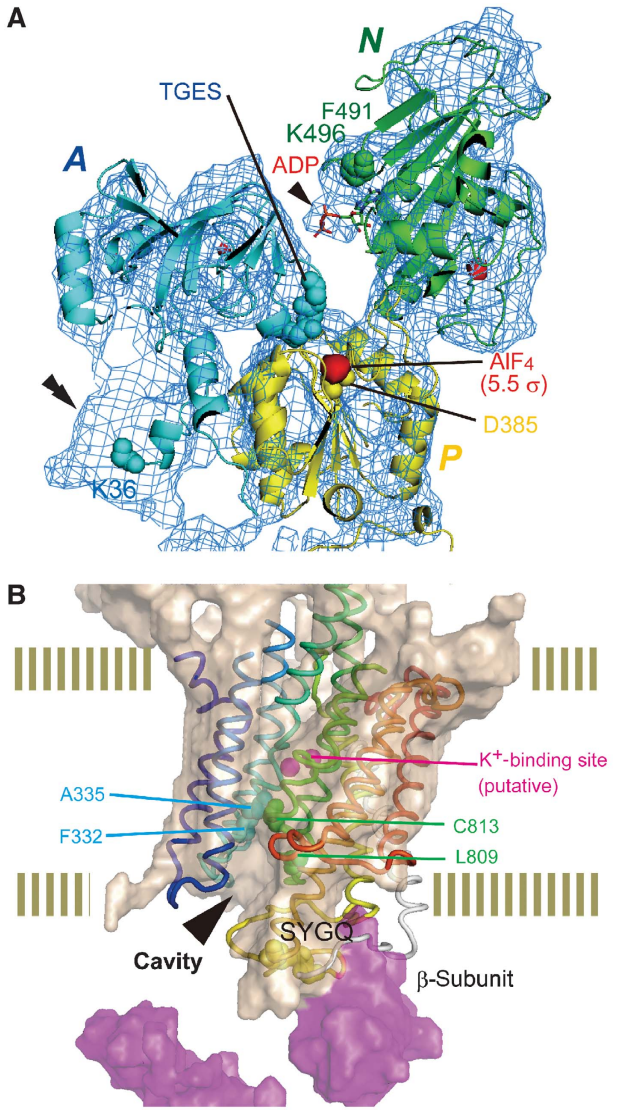

Figure 2 Architecture of the H^+,K^+-ATPase αβ-protomer in the pseudo-E_2P state. (**A**) Relative orientation of the cytoplasmic domains. The cytoplasmic domains of the homology model (in ribbon representation and colour coded as in Figure 1D) are superimposed on the density map contoured at 1.0 σ (blue mesh). A spherical density contoured at the 5.5 σ level (red) near the phosphorylation site (Asp 385) shows the position of the AlF_4 complex. The ADP molecule (stick representation) was fitted into the extra density found at the surface of the N domain (single arrowhead). The double arrowhead indicates the extra globular density found near the most N-terminal Lys 36 (blue sphere) in the homology model. Several key amino acids, including invariant ^{228}TGES motif, are shown in sphere representation. (**B**) Surface representation of the segmented map of the TM region of the α- (wheat) and β-subunit (magenta) contoured at 1.0 σ. The TM helices of the homology model of the α-subunit (coloured as in Figure 1D) and the β-subunit (white) are shown as tube models. The red spheres indicate the positions that correspond to bound Rb^+ in the Na^+,K^+-ATPase structure, showing the approximate locations of the cation-binding sites in the H^+,K^+-ATPase. The arrowhead indicates a funnel-like cavity that is surrounded by several amino acids important for inhibitor binding (shown as spheres). The conserved SYGQ sequence, which is critical for the assembly of the αβ-protomer, is shown as yellow spheres.

sites (e.g. Tyr9 by c-Src, Ser26 by PKC) and an ankyrin-binding site (Togawa *et al*, 1995; Kanagawa *et al*, 2000; Festy *et al*, 2001). This position of the N-terminus would allow for interactions with cytoplasmic proteins. A strong, spherical density peak exceeding a level of 5.5 σ can be seen at the position of the phosphorylating aspartate in the P domain (Asp385 in our model) and most likely represents the AlF_4 complex (Figure 2A). Moreover, a weak density protrudes from the N domain at a position close to two highly conserved residues, Phe491 and Lys496 in our model as shown by arrowhead in Figure 2A. Both residues are known to be important for the coordination of the adenine moiety (Teramachi *et al*, 2002). It is likely that this density represents ADP, which is bound in the low-affinity state and was also observed in the structure of SERCA in the E_2MgF state (Toyoshima *et al*, 2004). Thus, as observed earlier in the structure of SERCA in the E_2P state (Olesen *et al*, 2007), inclination of the P domain and penetration by the A domain's TGES loop cause the AlF_4 complex to be separated from the ADP molecule bound to the N domain. The AlF_4 complex is thus no longer accessible for coordination with ADP (Figure 2A).

The 10 TM helices (M1–M10) of the α-subunit and the additional TM helix of the β-subunit of our homology model are fit well into the TM part of the density map (Figure 2B). The putative cation-binding sites (Morth *et al*, 2007) are located in the middle of the TM region. Although these sites appear inaccessible from both sides of the membrane, a funnel-shaped cavity, formed by helices M4, M5, M8 and the luminal M5–M6 loop, extends from just beneath the ion-binding sites and opens into the luminal vestibule (arrowhead in Figure 2B). We assume that the reason why the ion-binding sites are not completely exposed to the luminal side is that our structure represents an E_2P transition state with bound AlF_4. As has been proposed for the SERCA E_2BeF_3 structure (Olesen *et al*, 2007), this cavity would presumably open upon transition to the E_2P ground state and expose the ion-binding sites to the lumen. Several residues located at the surface of the cavity (e.g. Phe332, Leu809 and Cys813) have been shown to be important for the binding of a K^+-competitive antagonist (Vagin *et al*, 2002; Munson *et al*, 2005). Cysteine 813 also forms a covalent bond with proton pump inhibitors such as omeprazole, used to treat gastric ulcers (Vagin *et al*, 2002). The cavity forming part of the cation transport pathway thus also contains binding sites for drugs. The structural features of the α-subunit described above are consistent with earlier studies, strongly supporting the reliability of our homology model based on the 6.5 Å map obtained by electron crystallography.

The β-subunit

In our EM map, the TM helix of the β-subunit (βTM) is represented by a cylindrical density next to helix M10 of the α-subunit (Figure 1D). Although there is clear density for the cytoplasmic half of βTM, density is missing for its luminal half. On the luminal side, the N-terminal region of the β-subunit ectodomain (Asano *et al*, 1999) appears to be in contact with the α-subunit, possibly through the conserved SYGQ sequence (Colonna *et al*, 1997) that was found to be critical for association of the β- with the α-subunit (Figure 2B). Despite rather low sequence identity (around 30%), the luminal β-subunit ectodomain appears similar to that of the Na^+,K^+-ATPase (Morth *et al*, 2007). It covers the luminal M7–M8 and M9–M10 loops of the α-subunit, which could explain the strong resistance of the

H^+,K^+-ATPase to both proteolysis and the highly acidic environment of the gastric lumen. At the same time, the vestibule between the luminal portion of the α-subunit and the β-subunit ectodomain would allow for efficient K^+ diffusion along the membrane surface (Miyazawa *et al*, 1999).

The cytoplasmic N-terminal tail of the β-subunit (βN) appears in the EM map as a continuous, rod-like density that connects between βTM and the α-subunit (Figure 3A and C). In contrast to the Na^+,K^+-ATPase structure, the N-terminal tail of the β-subunit is in contact with the outermost portion of the P domain (single arrowhead in Figure 3A and C) and the cytoplasmic end of M3 (double arrowhead in Figure 3A), respectively. Comparison of the SERCA structures in the E_1P-ADP and E_2P states revealed that the arrangement of the cytoplasmic domains is a key feature of the respective reaction state (Olesen *et al*, 2007). The interaction of βN with the P domain seen in our H^+,K^+-ATPase structure seems to stabilize the relative orientation of the cytoplasmic domains in the E_2P state, which would help to prevent the reverse reaction into the ADP-sensitive E_1P state and thus explain the preference of the H^+,K^+-ATPase for the E_2P state.

N-terminal deletion mutants of the β-subunit

To identify the possible function of βN, a series of N-terminal deletion mutants (Δ4, Δ8 and Δ13) was constructed and co-expressed with wild-type α-subunit in HEK-293 cells. Although several mutants expressed only at a rather low level, their specific activity and the amount of formed EP was proportional to their respective expression levels (data not shown). This finding suggests that, within the experimental error, wild-type and deletion mutants have the ATPase activity with the same turnover number and affinity for K^+ (Supplementary Figure S3A and B). Pulse-chase experiments with ^{32}P phosphoenzyme revealed, however, that the mutants differed significantly from wild-type H^+,K^+-ATPase in their distribution of EP in the E_1P and E_2P states (Figure 3B). E_1P and E_2P differ in their interaction with nucleotide and affinity for the transported cations (Figure 1A). In the E_1P state, the enzyme has a H^+ bound in an occluded state and it is ADP sensitive, that is, it can donate its phosphoryl group back to ADP to form ATP. The E_1P state is, therefore, known as a 'high energy' EP intermediate. In contrast, in the E_2P state, the enzyme is ADP insensitive, that is, it can only donate its phosphoryl group to water but not to ADP. The cation-binding site faces the lumen and has low affinity for

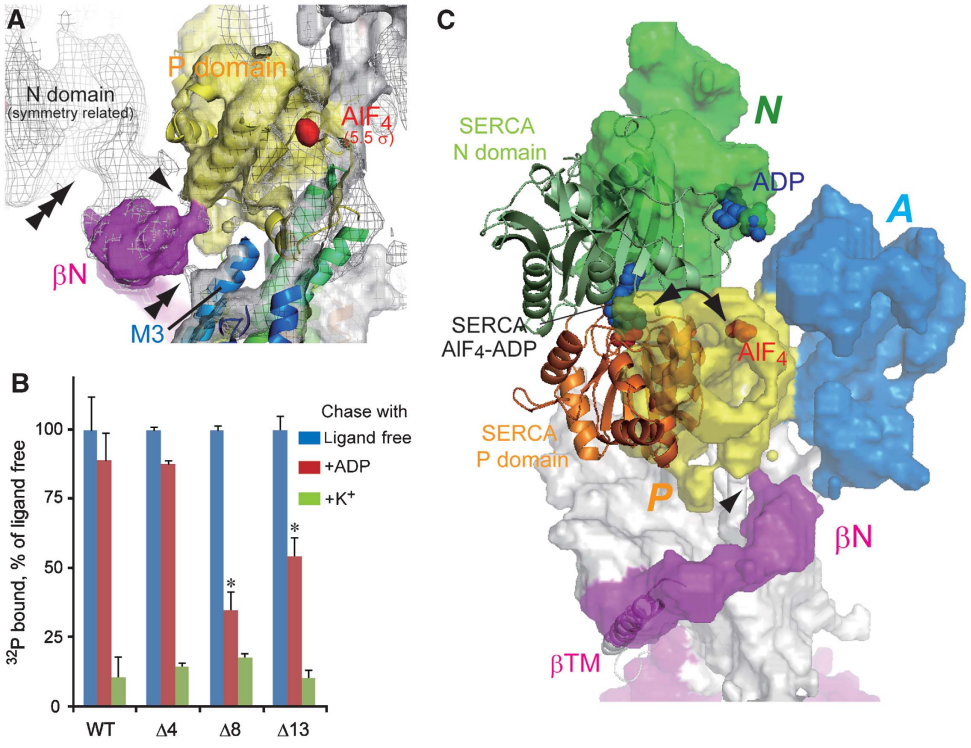

Figure 3 The N-terminal tail of the β-subunit functions as a ratchet. (**A**) Interaction between the α- and β-subunits. Segmented density map showing the P domain in yellow and the β-subunit in magenta. The single and double arrowheads indicate the position where the N-terminal tail of the β-subunit (βN) contacts the P domain and M3, respectively. The gray mesh represents the experimental density map including the symmetry-related molecule contoured at 1.0 σ. The triple arrowhead indicates the density that represents the N domain of the symmetry-related molecule. (**B**) ADP or K^+ sensitivity of the EP formed by βN deletion mutants. Pulse-chase experiments were performed on membrane fractions of wild-type (WT) and N-terminal deletion mutants (Δ4–Δ13) of the β-subunit co-expressed with wild-type α-subunit. The membrane fractions were phosphorylated for 10 s at 0°C with [γ-^{32}P]ATP. To measure dephosphorylation, the EP was chased with an excess of cold ATP to terminate phosphorylation from [γ-^{32}P]ATP, without (ligand free, blue) or with 1 mM ADP (+ADP, red) or 10 mM K^+ (+K^+, green), followed by acid quenching after 5 s of chasing (see Materials and methods). For each mutant, the phosphorylation level of the 'ligand-free' condition was assigned to 100%. Error bars show the standard deviation for three experiments. Asterisks indicate values significantly different from that of the wild-type one ($P<0.01$). (**C**) Comparison of the H^+,K^+-ATPase in the pseudo-E_2P state (surface representation as shown in Figure 1D) with SERCA in the E_1P-ADP state (ribbon model, PDB code 2ZBD). For clarity, the A domain and TM helices of SERCA are not shown. The two structures were aligned based on the M7–M10 segments. The ADP and AlF_4 molecules are shown as blue and red spheres, respectively.

H^+ but high affinity for K^+. In the E_2P state, the enzyme is K^+-sensitive, as binding of extracellular K^+ accelerates the hydrolysis of the bound phosphate. The difference in ADP sensitivity can be used to determine the relative amounts of E_1P and E_2P intermediates. Figure 3B shows the relative amount of EP after addition of unlabeled ATP to EP formed with [γ-^{32}P]ATP in the presence or absence of ADP or K^+ (see also Supplementary Figure S3C). For the β-subunit deletion mutants, which lack 8 (Δ8) or 13 (Δ13) amino acids from their N-terminus, the amount of EP is significantly reduced within 5 s after chasing with cold ATP and ADP. On the other hand, almost no effect was detected for the wild-type enzyme as well as the Δ4 mutant, which is consistent with the strong E_2P preference of gastric H^+,K^+-ATPase (Helmich-de Jong *et al*, 1985). These results show that gastric H^+,K^+-ATPase lacking βN is able to form an E_1P intermediate and can undergo the reverse reaction forming ATP from ADP (Rabon *et al*, 1982) ($E_2P \rightarrow E_1P + ADP \rightarrow E_1 + ATP$), thus losing its preference for the E_2P state, albeit under somewhat artificial conditions *in vitro*. In addition, all mutants show K^+ sensitivity. As every mutant exists in a dynamic equilibrium between the E_1P and E_2P states, stochastic fluctuations will sooner or later drive every H^+,K^+-ATPase molecule into the K^+-sensitive E_2P state, and thus render it susceptible to dephosphorylation in the presence of K^+. Therefore, our results suggest that βN truncations do not affect the forward reaction (E_1P to E_2P) but substantially accelerate the reverse reaction (E_2P to E_1P) due to destabilization of the E_2P state (see below).

βN involvement in the E_1P/E_2P equilibrium

The results of the deletion experiments indicate that the N-terminus of the β-subunit is involved in enzyme catalysis through its interaction with the catalytic domains of the α-subunit. This finding suggests that the observed inter-subunit contact of βN with the P domain of the α-subunit functions as a 'ratchet' that prevents the reverse reaction from the E_2P to the E_1P state by tethering the P domain in the E_2P-specific position. As described above, the reverse reaction from E_2P to E_1P is essentially prohibited in the case of gastric H^+,K^+-ATPase (Helmich-de Jong *et al*, 1985). Comparison of our pseudo-E_2P structure of H^+,K^+-ATPase with the E_1AlF_4-ADP structure of SERCA (Toyoshima *et al*, 2004) reveals a large movement of the P domain (Figure 3C). For the phosphorylation site, which in the E_2P state is obscured by the A domain (Figure 3C, surface representation), to become sensitive to ADP, the P domain needs to incline by $\sim 30^\circ$ away from βN, thus exposing its phosphorylation site to the ADP molecule bound to the N domain, as seen in the SERCA E_1P-ADP structure (Figure 3C, ribbon model). The interaction of βN with the P domain would counteract such a large domain reorganization and stabilize the position of the P domain, thus contributing to the inherent E_2P preference of the H^+,K^+-ATPase. Conversely, removal of βN would free the P domain and allow the bound phosphate molecule to react with the ADP in the N domain to form ATP.

Apart from the P domain, βN also appears to interact with the cytoplasmic portion of M3 (Figure 3A, double arrowhead). We cannot exclude the possibility that the A domain or other parts of the enzyme also contribute to the E_2P preference of the H^+,K^+-ATPase, in particular because it has been shown that the length of the A-M3 linker affects the E_1P–E_2P equilibrium in SERCA (Anthonisen EA and Andersen JP, 2008 P-ATPase conference). It is possible that βN interacts simultaneously with the P domain and M3. Although our homology model lacks 32 amino acids from βN, the rod-like density we assigned to βN would accommodate an α-helix of only $\sim$19 amino acids. The fold of βN may thus be more complex than it appears from its rod-like appearance in the EM map. Comparison of the amino-acid sequences of the N-terminal part of gastric H^+,K^+-ATPase β-subunit and kidney Na^+,K^+-ATPase β1-subunit reveals that β-subunit of H^+,K^+-ATPase has 5 amino acids longer than that of Na^+,K^+-ATPase. The results of our deletion experiment are suggestive of an important role for polar amino acids 5–8 at the N-terminus of the β-subunit (^{1}MAAL^{5}QEK^{8}K), although our 6.5 Å map could not discriminate any individual residues. The N-terminal 34 amino acids deletion of the Na^+,K^+-ATPase β-subunit has shown lower affinity for both Na^+ and K^+ than wild type, but not affected surface expression of the pumps (Geering *et al*, 1996; Hasler *et al*, 1998). A chimeric study of this portion showed that the N-terminal swapping gave a functional αβ-complex of H^+,K^+-ATPase with a slightly higher specific activity (Asano *et al*, 1999). Therefore, it would be interesting to perform an analysis of the E_1P/E_2P equilibrium for much shorter deletion of Na^+,K^+-ATPase β-subunit or its chimera with H^+,K^+-ATPase to understand the compatibility between closely related isoforms. Further point mutational analysis would also help to identify the specific interaction site, and to reduce possible secondary effects such as local misfolding. βN makes a crystal contact with the α-subunit of an αβ-complex in the adjoining membrane (Figure 3A, triple arrowhead), raising the possibility that the observed inter-subunit contact may be a crystallization artifact. We can exclude this possibility, however, because deletion of βN has a profound effect on the enzyme reactivity in solution.

We propose a novel molecular ratchet mechanism that explains the preference of the gastric H^+,K^+-ATPase for the E_2P state, which is likely to be relevant for the generation of a million-fold proton gradient across the gastric parietal cell membrane. We suggest that the observed interaction of βN with the P domain of the α-subunit leads to an energetically lower, stabilized E_2P state. The removal of βN would correspond to an increase in the energy level of the E_2P state and thus induce the reverse reaction through the E_1P intermediate, the energetically highest state in the reaction cycle. This notion is supported by the observed ADP sensitivity of the deletion mutants (Figure 3B). The reverse reaction could result in inefficient transport and, possibly, reverse flow of protons. The proposed ratchet mechanism would ensure that the transport cycle of the H^+,K^+-ATPase can only proceed in the forward direction. Although there is currently no information for the conformation of βN in other stages of the ion transport cycle, judged from the dephosphorylation of E_2P upon K^+ binding, the conformational change induced by the K^+ binding would be strong enough to allow the enzyme to proceed through the reaction cycle. However, for a full understanding of the ratchet mechanism, 3D structures of the gastric H^+,K^+-ATPase in other reaction states combined with further functional studies will be required.

Materials and methods

2D crystallization

Vesicles containing pig gastric H^+,K^+-ATPase (G1 fraction) were prepared (Sachs *et al*, 1976) and further purified with SDS (Yen *et al*, 1990) as described. The membrane fraction (2.5 mg/ml of protein), which shows >400 μmol P_i/mg/h specific ATPase activity (Abe *et al*, 2002), was solubilized for 10 min on ice with 0.25% (w/v) decylmaltoside in 40 mM MES, pH 5.5, 20 mM $Mg(CH_3CO_2)_2$, 5 mM ATP, 10% (w/v) glycerol. After removal of the insoluble material by ultracentrifugation at 186 000 *g* for 20 min, the supernatant was mixed with dioleoylphosphatidylcholine (Avanti) at a lipid-to-protein ratio (w/w) of 0.5. The samples were placed in 10 μl microdialysis buttons (Hampton Research) using a dialysis membrane with a molecular weight cut-off of 25 kDa (SPECTRA/Por #7, SPECTRUM). The sample was first dialyzed against 10 mM MES, pH 5.5, 1 mM $MgCl_2$, 0.5 mM $AlCl_3$, 4 mM NaF, 0.3 mM ADP, 3 mM DTT, 10% (w/v) glycerol at 0°C for 12 h and then against 20 mM propionate, pH 4.87, 1 mM $MgCl_2$, 0.5 mM $AlCl_3$, 4 mM NaF, 0.3 mM ADP, 3 mM DTT, 10% (w/v) glycerol at 3°C for 9–12 days.

Electron microscopy and image analysis

Samples were negatively stained with 2% (w/v) uranyl acetate to screen for crystals. For cryo-electron microscopy, 2D crystal samples were mixed with dialysis buffer containing 7–35% (w/v) trehalose, and prepared using the carbon sandwich method (Gyobu *et al*, 2004). After removal of excess buffer, the grid was blotted with filter paper and plunged into liquid nitrogen. All steps were performed at 4°C. Images were recorded with a JEM-3000SFF electron microscope (JEOL) equipped with a field emission gun and a super-fluid helium stage (Fujiyoshi *et al*, 1991) and operated at 300 kV. Images were recorded on SO-163 film (Kodak) at a nominal magnification of 40 000 ×, using a 2-s exposure and a total electron dose of 25 electrons/$Å^2$. The micrographs were developed for 14 min at 20°C using full-strength Kodak D19 developer. The quality of the images was assessed by optical diffraction, and selected images were digitized with a SCAI scanner (Zeiss) using a step size of 7 μm. The digitized images, typically 6000 × 6000 pixels, were processed with the MRC image processing programs (Crowther *et al*, 1996). The crystals were computationally unbent and corrected for the contrast transfer function (CTF) (Henderson *et al*, 1986). The initial CTF parameters for each image were determined by square frequency filtering (Tani *et al*, 1996) combined with periodogram averaging (Fernandez *et al*, 1997). The data from 346 images were combined using LATLINE (Agard, 1983) and used to calculate a density map. To objectively define the molecular boundaries of the H^+,K^+-ATPase, the program CODIV (Volkmann, 2002) was used to segment the density map and to extract an αβ-protomer. The EM density map has been deposited in the Electron Microscopy Data Bank (EMBD, http://www.ebi.ac.uk/msd-srv/emsearch/index.html, accession no 5104).

A multiple sequence alignment was carried out using ClustalW (Thompson *et al*, 1994) with minor manual adjustments based on secondary structure information for Na^+,K^+-ATPase and Ca^{2+}-ATPase. The homology model for the H^+,K^+-ATPase was built with MODELLER v9.2 (Šali and Blundell, 1993) using the atomic model of Na^+,K^+-ATPase (PDB code 3B8E) as the template. Initial manual fitting of the homology model into the density map was done in O (Jones *et al*, 1991), followed by fine adjustments for each individual domain structure using SITUS (Wriggers *et al*, 1999). After a positional search, the split loop regions were manually linked in O with regularization refinement. Figures were prepared with Pymol (http://pymol.sourceforge.net/). The coordinates of the homology model have been deposited in the Protein Data Bank (accession code 3IXZ).

Biochemical studies

Limited proteolysis with trypsin using purified membranes and crystallized samples was performed as described before (Nishizawa *et al*, 2008). Before tryptic digestion, membrane samples (0.5 mg/ml of protein) were incubated with the reaction conditions denoted in Supplementary Figure S2 for 30 min to 12 days at 4°C. Digestion was initiated by adding trypsin to the samples. The fragment patterns were analysed by SDS–PAGE using 10–20% polyacrylamide gradient gels (Supersep Ace, Wako, Japan). The gels were stained with Simply Blue SafeStain (Invitrogen).

Pulse-chase experiments were performed to analyse the EP states of the N-terminal deletion mutants of the β-subunit. The membrane fraction (Asano *et al*, 1996) (40 μg, permeabilized with 1 mM β-escin) of HEK-293 cells co-expressing wild-type α-subunit with wild-type or deletion mutants of the β-subunit was incubated for 10 s with 1 μM of [γ-^{32}P]ATP in the presence of 40 mM PIPES, pH 6.4, 10% glycerol, 20 μM $MgCl_2$, 1 mM ouabain in a volume of 40 μl. The phosphorylated enzymes were then chased by the addition of 160 μl of buffer containing 10 μM cold ATP, 40 mM PIPES, pH 6.4, 10% glycerol, 20 μM $MgCl_2$, without (ligand free) or with 1 mM ADP (+ADP), or 10 mM CH_3COOK (+K^+), respectively. The temperature was kept at 0°C throughout the entire reactions. After 5 s, 0.3 ml of 20% ice-cold trichloroacetic acid was added to terminate the reactions, and the amount of EP was determined using an earlier described assay to measure phosphorylation (Asano *et al*, 2001).

For the measurement of H^+,K^+-ATPase activity of HEK-293 cell expressing variants, the permeabilized membrane fraction (as described above) was incubated at 37°C with reaction buffer containing 40 mM PIPES, pH 7.0, 10% glycerol, 1 mM $MgCl_2$, 1 mM ATP and 2 mM or 0–50 mM CH_3CO_2K. After 10–20 min, the reaction was terminated by adding an equal volume of 12% SDS. The concentration of inorganic phosphate was determined colorimetrically by complexation with ammonium molybdate (Chifflet *et al*, 1988).

The turnover number is calculated as a ratio between the H^+,K^+-ATPase activity and the maximum amount of EP in each batch of membrane fractions. It is notable that each individual measurement for the ATPase activity and the amount of EP contains 3–5% error, suggesting that the scattered values found in Supplementary Figure S3A are largely due to the difference among membrane fractions. The values are normalized as a percent of wild type and presented as the mean value ± standard deviation for more than three independent experiments using different batch of membrane fractions (Vilsen, 1997).

Supplementary data

Supplementary data are available at *The EMBO Journal* Online (http://www.embojournal.org).

Acknowledgements

We thank Y Hiroaki and K Kobayashi (JEOL Datum) for help with sample preparation and electron microscopy. We are grateful to T Imagawa for the generous gift of pig gastric H^+,K^+-ATPase cDNA and K Taniguchi, T Friedrich, K Sakaguchi, S Kaya for valuable discussions. We also thank C Gerle, J Salje for critical reading of this manuscript. This research was supported by Grants-in Aid for Specially Promoted Research, the Global COE Program A06 to Kyoto University, and the Japan New Energy and Industrial Technology Development Organization (NEDO).

References

Abe K, Kaya S, Imagawa T, Taniguchi K (2002) Gastric H/K-ATPase liberates two moles of P_i from one mole of phosphoenzyme formed from a high-affinity ATP binding site and one mole of enzyme-bound ATP at the low-affinity site during cross-talk between catalytic subunits. *Biochemistry* **41:** 2438–2445

Agard DA (1983) A least-squares method for determining structure factors in three-dimensional tilted-view reconstructions. *J Mol Biol* **167:** 849–852

Asano S, Io T, Kimura T, Sakamoto S, Takeguchi N (2001) Alanine-scanning mutagenesis of the sixth transmembrane segment of gastric H^+,K^+-ATPase α-subunit. *J Biol Chem* **276:** 31265–31273

Asano S, Kimura T, Ueno S, Kawamura M, Takeguchi N (1999) Chimeric domain analysis of the compatibility between H^+,K^+-ATPase and Na^+,K^+-ATPase β-subunits for the functional expression of gastric H^+,K^+-ATPase. *J Biol Chem* **274:** 22257–22265

Asano S, Tega Y, Konishi K, Fujioka M, Takeguchi N (1996) Functional expression of gastric H^+,K^+-ATPase and site-directed mutagenesis of the putative cation binding site and the catalytic center. *J Biol Chem* **271:** 2740–2745

Chifflet S, Torriglia A, Chiesa R, Tolosa S (1988) A method for the determination of inorganic phosphate in the presence of labile organic phosphate and high concentrations of protein: application to lens ATPases. *Anal Biochem* **168:** 1–4

Chow DC, Forte JG (1995) Functional significance of the beta-subunit for heterodimeric P-type ATPases. *J Exp Biol* **198:** 1–17

Colonna TE, Huynh L, Fambrough DM (1997) Subunit interactions in the Na,K-ATPase explored with the yeast two-hybrid system. *J Biol Chem* **272:** 12366–12372

Crowther RA, Henderson R, Smith JM (1996) MRC image processing programs. *J Struct Biol* **116:** 9–16

Danko S, Yamasaki K, Daiho T, Suzuki H (2004) Distinct natures of beryllium fluoride-bound, aluminum fluoride-bound, and magnesium fluoride-bound stable analogues of an ADP-insensitive phosphoenzyme intermediate of sarcoplasmic reticulum Ca^{2+}-ATPase: changes in catalytic and transport sites during phosphoenzyme hydrolysis. *J Biol Chem* **279:** 14991–14998

Fernandez JJ, Sanjurjo JR, Carazo JM (1997) A spectral estimation approach to contrast transfer function detection in electron microscopy. *Ultramicroscopy* **68:** 267–295

Festy F, Robert JC, Brasseur R, Thomas A (2001) Interaction between the N-terminal domain of gastric H,K-ATPase and the spectrin binding domain of Ankyrin III. *J Biol Chem* **276:** 7721–7726

Fujiyoshi Y (1998) The structural study of membrane proteins by electron crystallography. *Adv Biophys* **35:** 25–80

Fujiyoshi Y, Mizusaki T, Morikawa K, Yamagishi H, Aoki Y, Kihara H, Harada Y (1991) Development of a superfluid helium stage for high-resolution electron microscopy. *Ultramicroscopy* **38:** 241–251

Ganser AL, Forte JG (1973) K^+-stimulated ATPase in purified microsomes of bullfrog oxynic cells. *Biochim Biophys Acta* **307:** 169–180

Geering K, Beggah A, Good P, Girardet S, Roy S, Schaer D, Jaunin P (1996) Oligomerization and maturation of Na,K-ATPase: functional interaction of the cytoplasmic NH_2 terminus of the β subunit with the α subunit. *J Cell Biol* **133:** 1193–1204

Gonen T, Cheng Y, Sliz P, Hiroaki Y, Fujiyoshi Y (2005) Lipid-protein interaction in double-layered two-dimensional AQP0 crystals. *Nature* **438:** 633–638

Gyobu N, Tani K, Hiroaki Y, Kamegawa A, Mitsuoka K, Fujiyoshi Y (2004) Improved specimen preparation for cryo-electron microscopy using a symmetric carbon sandwich technique. *J Struct Biol* **146:** 325–333

Hasler U, Wang X, Crambert G, Béguin P, Jaisser F, Horisberger JD, Geering K (1998) Role of β-subunit domains in the assembly, stable expression, intracellular routing, and functional properties of Na,K-ATPase. *J Biol Chem* **273:** 30826–30835

Helmich-de Jong ML, van Emst-de Vries SE, De Pont JJ, Schuurmans Stekhoven FM, Bonting SL (1985) Direct evidence for an ADP-sensitive phosphointermadiate of $(K^+ + H^+)$-ATPase. *Biochim Biophys Acta* **821:** 377–383

Henderson R, Baldwin JM, Downing KH, Lepault J, Zemlin F (1986) Structure of purple membrane from Halobacterium halobium: recording, measurement and evaluation of electron micrographs at 3.5 Å resolution. *Ultramicroscopy* **19:** 147–178

Jones TA, Zou JY, Cowan SW, Kjeldgaard M (1991) Improved methods for building protein models in electron density maps and the location of errors in these models. *Acta Crystallogr A* **47:** 110–119

Kanagawa M, Watanabe S, Kaya S, Togawa T, Imagawa T, Shimada A, Kikuchi K, Taniguchi K (2000) Membrane enzyme systems responsible for the Ca^{2+}-dependent phosphorylation of Ser^{27}, the independent phosphorylation of Tyr^{10} and Tyr^{7}, and the dephosphorylation of these phosphorylated residues in the α-chain of H/K-ATPase. *J Biochem* **127:** 821–828

Miyazawa A, Fujiyoshi Y, Stowell M, Unwin N (1999) Nicotinic acetylcholine receptor at 4.6 Å resolution: transverse tunnels in the channel wall. *J Mol Biol* **288:** 765–786

Miyazawa A, Fujiyoshi Y, Unwin N (2003) Structure and gating mechanism of the acetylcholine receptor pore. *Nature* **423: 949–955**

Morth JP, Poulsen H, Toustrup-Jensen MS, Schack VR, Egebjerg J, Andersen JP, Vilsen B, Nissen P (2007) Crystal structure of the sodium-potassium pump. *Nature* **450:** 1043–1049

Munson K, Garcia R, Sachs G (2005) Inhibitor and ion binding sites on the gastric H,K-ATPase. *Biochemistry* **44:** 5267–5284

Nishizawa T, Abe K, Tani K, Fujiyoshi Y (2008) Structural analysis of 2D crystals of gastric H^+,K^+-ATPase in different states of the transport cycle. *J Struct Biol* **162:** 219–228

Olesen C, Picard M, Winther AM, Gyrup C, Morth JP, Oxvig C, Møller JV, Nissen P (2007) The structural basis of calcium transport by the calcium pump. *Nature* **450:** 1036–1042

Palmgren MG, Axelsen KB (1998) Evolution of P-type ATPases. *Biochim Biophys Acta* **1365:** 37–45

Pedersen BP, Buch-Pedersen MJ, Morth JP, Palmgren MG, Nissen P (2007) Crystal structure of the plasma membrane proton pump. *Nature* **450:** 1111–1114

Post RL, Kume S (1973) Evidence for an aspartyl phosphate residue at the active site of sodium and potassium ion transport adenosine triphosphatase. *J Biol Chem* **248:** 6993–7000

Rabon E, Sachs G, Mårdh S, Wallmark B (1982) ATP/ADP exchange activity of gastric $(H^+ + K^+)$-ATPase. *Biochim Biophys Acta* **688:** 515–524

Rabon EC, Reuben MA (1990) The mechanism and structure of the gastric H,K-ATPase. *Annu Rev Physiol* **52:** 321–344

Sachs G, Chang HH, Rabon E, Schackman R, Lewin M, Saccomani G (1976) A nonelectrogenic H^+ pump in plasma membrane of hog stomach. *J Biol Chem* **251:** 7690–7698

Šali A, Blundell TL (1993) Comparative protein modeling by satisfaction of spatial restraints. *J Mol Biol* **234:** 779–815

Tani K, Sasabe H, Toyoshima C (1996) A set of computer programs for determining defocus and astigmatism in electron images. *Ultramicroscopy* **65:** 31–44

Teramachi S, Imagawa T, Kaya S, Taniguchi K (2002) Replacement of several single amino acid side chains exposed to the inside of the ATP-binding pocket induces different extents of affinity change in the high and low affinity ATP-binding sites of rat Na/K-ATPase. *J Biol Chem* **277:** 37394–37400

Thompson JD, Higgins DG, Gibson TJ (1994) CLUSTAL W: improving the sensitivity of progressive multiple sequence alignment through sequence weighting, position-specific gap penalties and weight matrix choice. *Nucleic Acids Res* **22:** 4673–4680

Togawa K, Ishiguro T, Kaya S, Shimada A, Imagawa T, Taniguchi K (1995) Reversible phosphorylation of both Tyr7 and Tyr10 in the α-chain of pig stomach H^+,K^+-ATPase by a membrane-bound kinase and a phosphatase. *J Biol Chem* **270:** 15475–15478

Toyoshima C, Nakasako M, Nomura H, Ogawa H (2000) Crystal structure of the calcium pump of sarcoplasmic reticulum at 2.6 Å resolution. *Nature* **405:** 647–655

Toyoshima C, Nomura H, Tsuda T (2004) Luminal gating mechanism revealed in calcium pump crystal structures with phosphate analogues. *Nature* **432:** 361–368

Vagin O, Denevich S, Munson K, Sachs G (2002) SCH28080, a K^+-competitive inhibitor of the gastric H,K-ATPase, binds near the M5-6 luminal loop, preventing K^+ access to the ion binding domain. *Biochemistry* **41:** 12755–12762

Vilsen B (1997) Leucine 332 at the boundary between the fourth transmembrane segment and the cytoplasmic domain of Na^+,K^+-ATPase plays a pivotal role in the ion translocating conformational changes. *Biochemistry* **36:** 13312–13324

Volkmann NA (2002) Novel three-dimensional variant of the watershed transform for segmentation of electron density maps. *J Struct Biol* **138:** 123–129

Wolosin JM (1985) Ion transport studies with H^+-K^+-ATPase-rich vesicles: implications for HCl secretion and parietal cell physiology. *Am J Physiol* **248:** G595–G607

Wriggers W, Milligan RA, McCammon JA (1999) Situs: a package for docking crystal structures into low-resolution maps from electron microscopy. *J Struct Biol* **125:** 185–195

Yen LA, Cosgrove P, Holt W (1990) SDS purification of porcine H,K-ATPase from gastric mucosa. *Membr Biochem* **9:** 129–140

Zhang P, Toyoshima C, Yonekura K, Green NM, Stokes DL (1998) Structure of the calcium pump from sarcoplasmic reticulum at 8-Å resolution. *Nature* **392:** 835–839